AIAA 2002-4700

X-33 Turbulent Aeroheating Measurements and Predictions

Brian R. Hollis, Scott A. Berry, and Thomas J. Horvath
NASA Langley Research Center
Hampton, VA

AIAA Atmospheric Flight Mechanics Conference and Exhibit
05-08 August 2002
Monterey, California

X-33 Turbulent Aeroheating Predictions and Measurements

Brian R. Hollis*, Scott A. Berry†, and Thomas J. Horvath†
NASA Langley Research Center, Hampton, VA 23681

Measurements and predictions of the X-33 turbulent aeroheating environment have been performed for Mach 6, perfect-gas air conditions. The purpose of this investigation was to compare turbulent aeroheating predictions from two Navier-Stokes codes, LAURA and GASP, with each other and with experimental data in which turbulent flow was produced through either natural transition or forced transition using roughness elements. The wind tunnel testing was conducted at free stream Reynolds numbers of 0.72 x 10^7/m to 2.4 x 10^7/m (2.2 x 10^6/ft to 7.3 x 10^6/ft) on 0.254 m (10.0-in.) X-33 models at α = 40-deg with smooth surfaces, smooth surfaces with discrete trips, and surfaces with simulated bowed thermal protection system panels. Turbulent flow was produced by the discrete trips and bowed panels for all but the lowest Reynolds number, while turbulent flow on the smooth model was produced only at the highest Reynolds number. Turbulent aeroheating levels on each of the three model types were measured using global phosphor thermography and agreed to within the experimental accuracy (±15%) of the test technique. Computations were performed at the wind tunnel free stream conditions using both codes. Turbulent aeroheating levels predicted using the LAURA code were generally 5%-10% lower than those from GASP, although both sets of predictions fell within the experimental accuracy of the wind tunnel data.

Nomenclature

H_{AW}	adiabatic wall enthalpy (J/kg)
H_w	wall enthalpy (J/kg)
H_0	total enthalpy (J/kg)
h	heat transfer coefficient (kg/m^2/sec), $h = q/(H_{AW} - H_w)$
h_{FR}	reference Fay-Riddell heat transfer coefficient (kg/m^2/sec)
L	model reference length (m)
M_∞	free stream Mach number
q_{FR}	reference Fay-Riddell heat transfer rate (W/m^2)
Re_∞	free stream unit Reynolds number (1/m)
T_∞	free stream temperature (K)
U_∞	free stream velocity (m/sec)
α	angle-of-attack (deg)
X	streamwise distance coordinate from nose (m)
ρ_∞	free stream density (kg/m^3)

* Aerospace Technologist, Senior Member AIAA
† Aerospace Technologist

Introduction

The turbulent aeroheating environment of a proposed reusable launch vehicle (RLV) has been investigated through both experimental and computational methods. The purpose of this investigation was to compare turbulent heating levels predicted using two commonly-used Navier-Stokes codes, LAURA and GASP, with each other and with wind tunnel data. The X-33 vehicle, which was intended to be a sub-scale technology demonstrator for an economical, full-scale, Single-Stage-to-Orbit Reusable Launch Vehicle (SSTO-RLV)[1-5] was selected as the basis for this study. Although the future of the program is currently in doubt, a large experimental/computational aerothermodynamic database[6-17] was developed by NASA for the X-33, and a considerable investment was made to produce computational surface geometries and grids and to design and fabricate wind tunnel models. Therefore, the X-33 configuration was an ideal choice for this study.

While previously reported X-33 turbulent aeroheating comparisons[10] were limited to a single free stream Reynolds number of $3.3x10^6$ (based on model length), the current work extends both measurements and predictions to a wider Reynolds number range of $1.8x10^6$ to $6.1x10^6$ with turbulent boundary layer flow due to either natural transition or to forced transition by discrete or distributed roughness elements. Previously noted differences[10] in turbulent data from discrete and distributed roughness elements are also addressed and are shown to be due to calibration error.

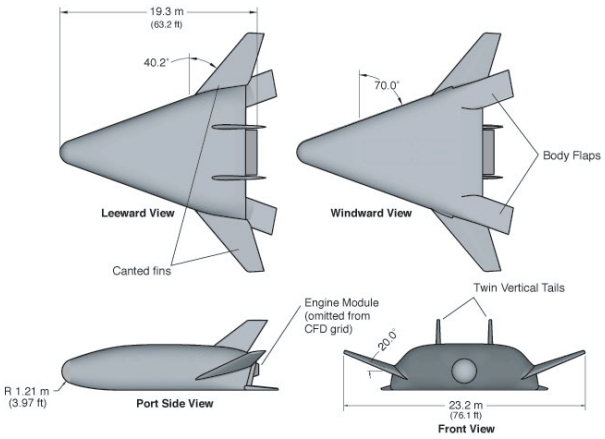

Figure 1: Dimensioned Sketch of Full-Scale X-33 F-Loft, Rev-F Configuration

Figure 2: NASA LaRC 20-Inch Mach 6 Air Tunnel

X-33 Vehicle Geometry

The computational results presented in this reference are based on the 604B0002F configuration of the Lockheed-Martin X–33 vehicle, which is commonly referred to as the F–Loft, Rev–F configuration. This configuration (Fig. 1) is a lifting-body delta planform with twin vertical tails, canted fins and body flaps. The body length is 19.3 m (63.2 ft.) from the nose to the end of the engine module, and the span across the canted fins is 23.2 m (76.1 ft). The canted fins have a dihedral of 20-deg and a -8.58-deg incidence angle.

Experimental Method

Test Facility

Aeroheating tests were conducted in the NASA LaRC 20-Inch Mach 6 Air Tunnel. This facility is a blow-down tunnel in which heated, dried, and filtered air is used as the test gas. The tunnel has a two dimensional, contoured nozzle which opens into a 0.521 m x 0.508 m (20.5-in. x 20.0-in.) test section. The tunnel is equipped with a bottom-mounted injection system which can transfer a model from the sheltered model box to the tunnel centerline in less than 0.5 sec. Run times of up to 15 minutes are possible in this facility, although for aeroheating studies only a few seconds of model exposure to the flow are required to perform measurements. The nominal reservoir conditions of this facility are stagnation pressures of 206.8 to 3447.4 kPa (30 to 500 psia) with stagnation temperatures of 422.2 to 555.5 K (760 ˚R to 1000 ˚R), which produce perfect-gas free stream flows with Mach numbers between 5.8 and 6.1 and Reynolds numbers of $1.64x10^6$/m to $23.3x10^6$/m ($0.5x10^6$/ft to $7.3x10^6$/ft). A more detailed description of this facility is presented in Refs. 18 and 19. Representative flow conditions for each of the standard 20-Inch Mach 6 Air Tunnel operating points at which tests were conducted have been computed using the GASPROPS (Ref. 20) code and are listed in Table 1.

Measurement Technique

Global surface heating distributions were obtained using the digital optical measurement method of two color, relative-intensity, phosphor thermography (Refs. 21-24). In this method, ceramic wind tunnel models are coated with a phosphor compound which fluoresces in two separate regions (green and red) of the visible light spectrum. Before and during a wind tunnel run, the phosphor-coated model is illuminated by ultraviolet (UV) light sources, and the resulting fluorescent intensity of the model is recorded and digitized through a three-color CCD (charge coupled device) camera. Intensity data are converted to surface temperature values using system calibrations. Global heat-transfer distributions are then computed from these temperature data using one-dimensional, constant heat-transfer coefficient conduction theory. As discussed in Ref. 10, the estimated experimental uncertainty of the heating data is approximately ±15%.

The heating data are presented in the non-dimensional form, h/h_{FR}, where h_{FR} is the reference heat-transfer coefficient from Fay-Riddell theory (Ref. 25) for a 300 K (540 ˚R) surface temperature and a radius of 1.60 cm (0.630-in.), which is approximately that of the nose of the X-33 models. In the definitions of both h and h_{FR}, the adiabatic wall enthalpy, H_{AW}, is assumed to be equal to the total enthalpy, H_0.

Wind Tunnel Models

Cast ceramic models are used for aeroheating testing with the thermographic phosphor system. To fabricate these models, a rapid prototyping stereolitho-

Table 1: Wind Tunnel Free Stream Conditions

Operating Condition	M_∞	T_∞ (K)	ρ_∞ (kg/m^3)	U_∞ (m/s)	h_{FR} (kg/m^2/s)	q_{FR} (W/cm^2)
$Re_\infty = 0.72\text{x}10^7$/m	5.95	62.4	$3.343\text{x}10^{-2}$	942.0	0.3944	8.103
$Re_\infty = 1.4\text{x}10^7$/m	6.00	61.5	$6.438\text{x}10^{-2}$	941.7	0.5470	11.67
$Re_\infty = 1.9\text{x}10^7$/m	6.03	62.6	$8.953\text{x}10^{-2}$	953.3	0.6548	14.16
$Re_\infty = 2.4\text{x}10^7$/m	6.06	62.4	$1.136\text{x}10^{-1}$	955.6	0.7397	16.14

graphic apparatus is first used to build a resin model of the configuration. A wax mold of the resin model is then formed, and then a patented silica-ceramic investment slip-casting technique is used to make a ceramic shell model of the vehicle. The ceramic shell model is backfilled with a hydraulically setting magnesia ceramic for strength and support into which a sting is fixed. Finally, the model is coated with a mixture of phosphors suspended in a silica-based colloidal binder.

The model scale was 0.0132, which resulted in a 0.254 m (10.0-in.) model length measured from the nose to the end of the engine module. The effects of raised or bowed thermal protection system (TPS) tiles on the state of the boundary layer were investigated through the use of discrete and distributed roughness elements. Discrete roughness elements were produced by application of 0.064 mm to 0.17 mm (0.0025-in. to 0.0065-in) height squares of polyimide film (either a single element on the centerline or a spanwise array of elements across the body) at an X/L location of 0.20 on the windward surface of a model (Fig. 3). A distributed roughness pattern which simulated the bowing of the windward surface TPS tiles due to temperature gradients within the metallic tiles was created through fabrication of models (Fig. 4) with tiles raised to heights of 0.15 mm (0.0060-in.) from X/L = 0.10 to 0.45. In comparison to the trip or bowed panel heights, the surface roughness of the phosphor coating has been measured to be approximately 0.013 mm (0.0005-in.). Further details on the roughness elements can be found in Ref. 8.

Computational Method

Numerical Algorithms

Perfect-gas air, turbulent aeroheating computations were performed at the wind tunnel test conditions using two Navier-Stokes solvers, LAURA (v. 4.9.2) and GASP (v. 3.2.3). Free stream conditions for the computations were set to the nominal operating conditions of the NASA Langley Research Center (LaRC) 20-Inch Mach 6 Air Tunnel, which are listed in Table 1. For these computations, a uniform, ambient 300 K wall temperature boundary condition was imposed. The use of a constant wall temperature was valid because the experimental data were reported in terms of the non-dimensional ratio, h/h_{FR}, which is assumed to remain constant with wall temperature.

Figure 3: Close-up of Trip Array Near Nose

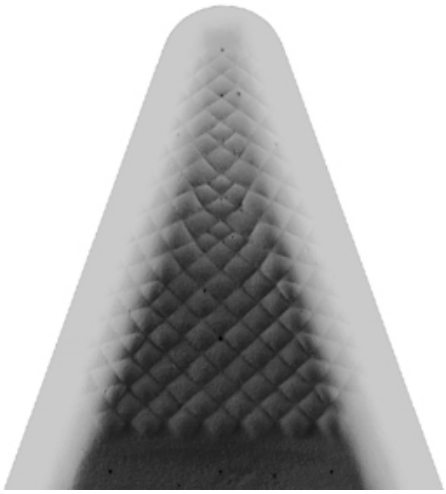

Figure 4: Close-up of Bowed Panels in Nose Region

The LAURA (Langley Aerothermodynamic Upwind Relaxation Algorithm) code (Refs. 26 and 27) is a three-dimensional, finite-volume solver which includes perfect-gas, equilibrium, and non-equilibrium chemistry models. The code can be used to solve the inviscid, thin-layer Navier-Stokes, or full Navier-Stokes equations. In the current study the thin-layer mode was employed; this mode has been shown (e.g. Ref. 28) to produce accurate results for attached flows at a considerable savings in computational time requirements. Time integration to steady-state in LAURA is accomplished through a point-relaxation scheme. Roe-averaging (Ref. 29) with Harten's entropy fix (Ref. 30) and Yee's Symmetric Total Variation Diminishing limiter (Ref. 31) is used for inviscid fluxes, and a second-order scheme is employed for viscous fluxes. For turbulent computations, the algebraic Baldwin-Lomax (Ref. 32) model with modifications (Ref. 33) for compressible flow and the Dhawan-Narashima (Ref. 34) transition model were employed.

The GASP (General Aerodynamic Simulation Program) code (Ref. 35) is a three-dimensional, finite-volume Navier-Stokes solver which incorporates numerous flux formulations, thermochemical models, turbulence models, and time-integration methods. The perfect-gas air model was used for these computations. The Jacobi scheme was used for time-integration. Full viscous terms were retained for all three directions and modeled with second-order central differences. As described in Ref. 10, a third-order, upwind biased, min-mod limited scheme, which consisted of a Roe flux formulation in the body-normal direction and a van Leer formulation in the other two directions, was employed to represent the inviscid fluxes and was found to produce the most accurate heat-transfer results. The turbulent computations were performed using the algebraic Baldwin-Lomax model, which was modified for this study with the same compressibility correction as in the LAURA code (Ref. 33).

Grid Adaptation and Convergence

Computations were performed on single-block grids at model scale with a density of 127 streamwise points, 181 circumferential points, and 33, 65, or 129 body-normal points. During a computation, the grid was adapted to align the outer boundary of the grid with the bow shock and to cluster points in the wall boundary layer. Typically, the outer boundary was adjusted so that the shock was at approximately 80% of the normal distance from the wall to the outer grid boundary and the wall cell Reynolds numbers were in the range of 1 to 10.

Grid adaptation was performed using the scheme detailed in Ref. 27. This scheme is internal to the LAURA code, but a separate external code had to be developed to post-process GASP solution files for grid adaptation using this method. Solution files were output from GASP at regular intervals, adapted, and then read back into GASP, and iteration toward a final solution was continued. Because of the time required to export, post-process, and re-import solution data, the number of grid adaptations in a GASP solution was usually less than for a LAURA solution. As a result, grids in LAURA solutions were generally smoother, and thus solution convergence was more rapid. When the more limited number of grid adaptations in the GASP solutions did not produce a suitably smooth grid, the VGM (Volume Grid Manipulation) code (Ref. 36) was used to provide additional smoothing.

Because of the different grid adaptation procedures followed with GASP and LAURA, grid adaptation must be considered as one of the variables in the comparison of results between the two codes. Although code-to-code comparisons often are performed on a one-to-one basis (i.e. identical grids), it was decided that since grid adaption is internal to the LAURA code, and thus an intrinsic contributor to the final solution, a more realistic comparison would be obtained using the different grids which were produced by the two codes.

In the previous study (Ref. 10) a 127 x 181 x 65-point grid was used to perform laminar, perfect-gas computations with the GASP code. A grid-convergence study demonstrated that for this resolution, the grid-convergence error was approximately 2-3% over most the vehicle for laminar computations. LAURA results would be expected to be the same or better, given the better grid adaption capability in that code.

For the current turbulent aeroheating study, the normal grid resolution was varied from 33 to 129 points. Results for GASP computations were performed for the $Re_\infty = 2.4x10^7$/m case with 33, 65, and 129 normal points are shown in Fig. 5. Centerline heating levels dropped by approximately 10% from the 33-point grid to the 65-point grid, and dropped by approximately 5% from the 65-point grid to the 129-point grid. Based on these results, all further GASP computations were performed on 129-point grids, and the grid convergence error for the GASP computations was estimated as 5%. A smaller change grid convergence error would have been desirable, but further grid resolution increases were impractical from the standpoint of computational resources. Results for LAURA computations at the same condition are shown in Fig. 6. LAURA heating levels dropped by only 2% (except near the nose) between the 33-point and 65-point grids; therefore further grid resolution increases were not deemed necessary and all LAURA computations were performed on 65-point grids.

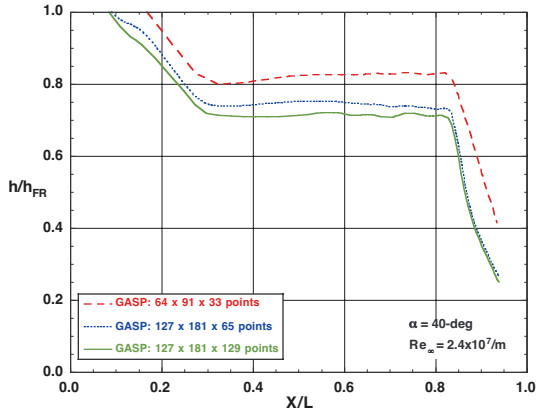

Figure 5: Turbulent Centerline Heating Levels Computed with GASP for Different Grid Resolutions

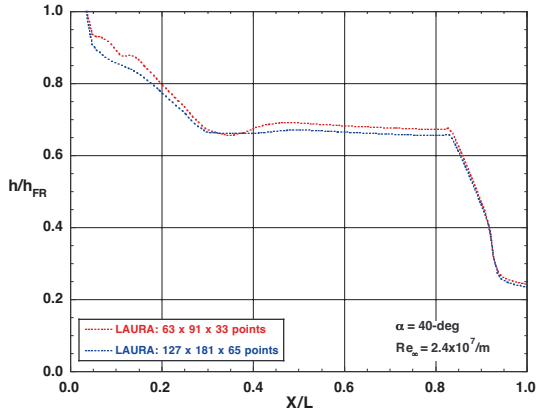

Figure 6: Turbulent Centerline Heating Levels Computed with LAURA for Different Grid Resolutions

The difference in grid resolution requirements for GASP and LAURA solutions was attributed to two possible factors: grid quality and algorithm accuracy. As mentioned earlier in this section, LAURA solutions were computed with a greater number of grid adaptations than GASP solutions, and this fact probably contributed to the final quality of the converged solution. In regard to the accuracy of the algorithm, it was shown (after these GASP computations had been completed) in Ref. 16 that the "minmod" limiter in the version of GASP employed in this study (v 3.2.3) contains a factor that increases the stability of the computation at the cost of increased numerical dissipation and for laminar computations can produce higher heating levels than would normally be expected. While for turbulent computations the effects of this increased dissipation are small relative to the turbulent viscosity, a slight effect on heating levels might still be expected.

Experimental and Computational Results and Comparisons

Comparison of Current and Previously Reported Experimental Heating Data

In previously reported comparisons (Ref. 10) of predicted and measured X-33 heating levels, it was noted that turbulent heating levels produced by discrete and distributed roughness elements differed by up to 30%. The distributed roughness heating levels (from bowed panel models) compared well (±10%) with the computed turbulent heating distributions (from GASP solutions) but the discrete roughness heating levels (from smooth models with trips) were up to 20% lower than the predictions. The reason for this difference was not resolved at that time, and addressing this problem was the first step in the experimental phase of this study.

The experiments reported in Refs. 8 and 12 were repeated for the selected test case of α = 40-deg at $Re_\infty = 1.4x10^7$/m. Existing smooth and bowed-panel models as well as newly-fabricated smooth and bowed panel models were tested in the current study.

Centerline heating comparisons of the original test data with new test data obtained on both original and new models are presented in Fig. 7 for the smooth models, in Fig. 8 for the bowed panel models, and in Fig. 9 for smooth models with a 0.13 mm (0.0050-in.) trip on the centerline at X/L = 0.20. As shown in these figures, both the smooth model (without trip) and bowed panel model heating measurements were repeatable (Figs. 7 and 8) to within the experimental uncertainty. However, for the smooth models with trips (Fig. 9), the data on the new model were up to 40% higher than the original data (note that the original smooth model was damaged during testing before the discrete trip test could be repeated on it).

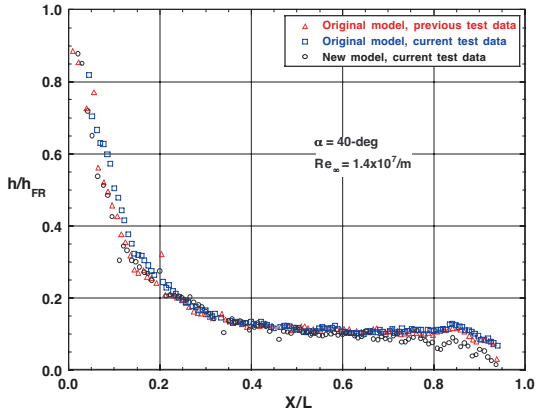

Figure 7: Comparison of Centerline Heating Data for Smooth Model

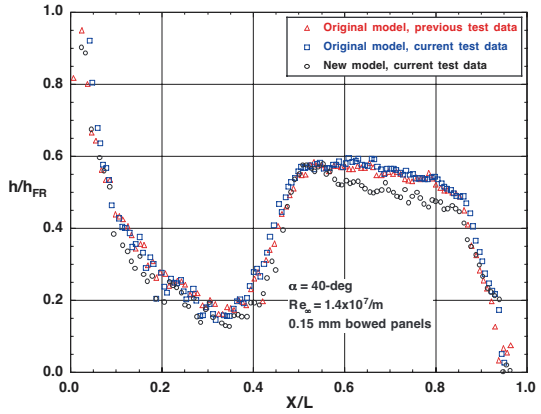

Figure 8: Comparison of Centerline Heating Data for 0.15 mm Bowed Panel Models

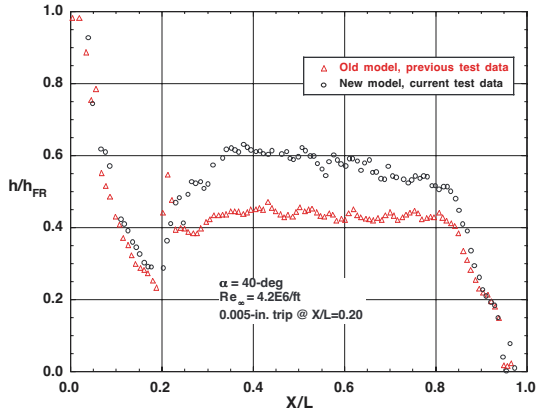

Figure 9: Comparison of Centerline Heating Data for Smooth Model With 0.13 mm Trip

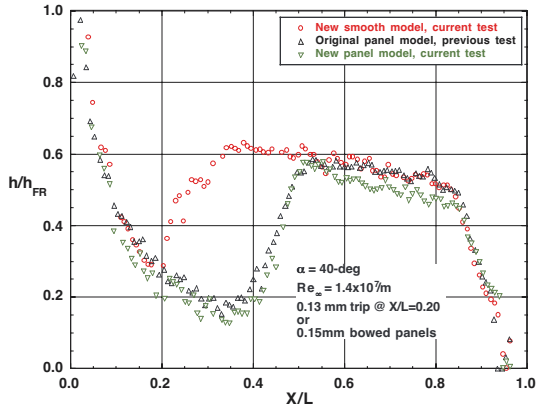

Figure 10: New Comparison of Centerline Heating Data for Trip and Bowed Panel Model s

The differences in the measured heating levels on the smooth model with a discrete trip prompted a thorough re-examination of the original data and the methodology used to obtain those data. It was found that incorrect calibration data had been input into the data acquisition system during several of the previous X-33 heating tests, and as a result the model surface temperatures, and thus the magnitudes of the surface heating distributions, were computed incorrectly from the raw data. This calibration error affected all tests in which discrete-trip heating measurements were made, while smooth and bowed-panel heating tests were conducted either before this error or in subsequent tests in which the correct calibration data were input. The effect of this calibration error increased with temperature; thus, turbulent heating levels due to discrete trips were significantly under-estimated, but the error in the lower, laminar heating levels was small.

Thus, smooth and bowed panel data reported in Refs. 8, 10, and 12 were correct, but the discrete trip data were incorrect, and so, therefore, was the observation that the trips and bowed panels produced turbulent heating levels which differed by large amounts.

For the range of roughness element heights considered in the current study, discrete trip turbulent heating levels were found to differ from the bowed panel data by ±2% at the least and by +10% at the most. A sample comparison is shown in Fig. 10 for Re_∞ = $1.4x10^7$/m. While differences were observed across the test Reynolds number range, they were within the estimated ±15% uncertainty. Thus, these difference could be attributable to other systemic factors such as the accuracy in casting the aerolines of the different ceramic models, the quality of the thermographic phosphor coating of the different models, etc. Therefore, it is concluded that any differences in heating levels due to the two different tripping mechanisms were smaller than the experimental uncertainty.

In regard to the calibration error discovered in the original data, it is important to note that the main purpose of the prior X-33 experimental aeroheating research was to determine boundary layer transition criteria, while measurement of heating levels was a secondary goal. Although this calibration error led to incorrect measurements of heating levels, it did not affect the character of the data - i.e. the measured location of transition onset or the growth of the area covered by the turbulent wedge downstream of transition. The transition criteria reported in Ref. 8 thus remain valid.

Effect of Discrete Trip Height on Heating Levels

As part of the investigation into the differences between discrete and distributed roughness turbulent heating levels observed in the older data, tests were conducted with various trip heights to determine if this

parameter influenced the heating levels. Runs were made at $\alpha = 40$-deg at $Re_\infty = 1.4x10^7$/m with single trips of 0.064 mm to 0.15 mm (0.0025-in. to 0.0065-in.) height placed on the centerline at $X/L = 0.20$. Results are shown in Fig. 11. For trip heights of 0.089 mm (0.0035-in.), 0.13 mm (0.0050-in.), and 0.15 mm (0.0065-in.), the flow field disturbance caused by the trip produced a short region of transitional flow ($X/L \sim$ 0.20 to 0.40) followed by apparently fully-developed turbulent flow. For these trips heights, there was only a small difference in transition length, and heating levels downstream of transition agreed closely. In contrast, the disturbance caused by the 0.064 mm (0.0025-in.) trip led to a long region of transitional flow which did not appear to ever reach a completely turbulent state.

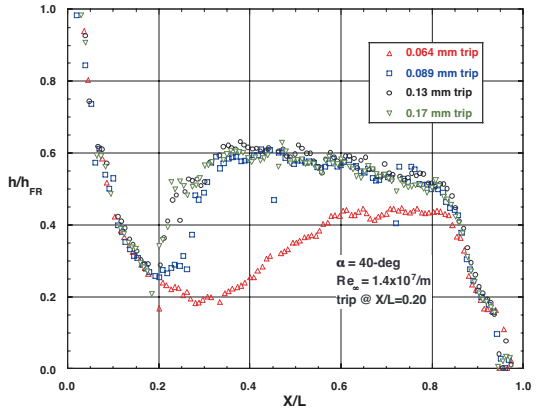

Figure 11: Effect of Trip Height on Centerline Heating Levels at $Re_\infty = 1.4x10^7$/m

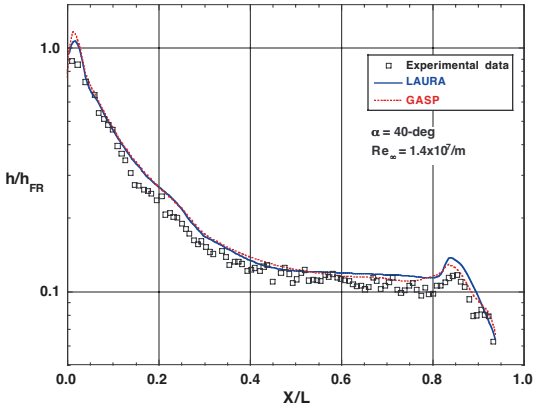

Figure 12: Laminar Centerline Heating Comparison Between Measurements and Predictions at $Re_\infty = 1.4x10^7$/m

Comparison of Predicted and Measured Heating Levels

Before comparisons of turbulent measurements and predictions are considered, a laminar comparison is shown in Fig. 12 to demonstrate the baseline agreement between experiment and computations. Except near the nose stagnation point, predicted heating levels from the two codes agreed to within 5% and the experimental data agreed with the predictions to within the ±15% experimental uncertainty.

Comparisons of measured and predicted centerline turbulent heating levels are shown for each of the four test Reynolds numbers in Figs. 13-16. To generate the discrete trip data shown in these figures, an array of nine 0.17mm (0.0065-in.) trips which spanned the body at $X/L = 0.20$ was used (as shown in Fig. 3).

The smooth model without trips produced fully-turbulent flow only at the highest test Reynolds number (Fig. 16), while the models with trips and bowed panels produced turbulent flow at all but the lowest Reynolds number (Fig. 14-16) although the transition onset locations differed between the two tripping methods. At the lowest Reynolds number (Fig. 13), turbulent flow was produced only when a discrete trip was added to a bowed-panel model. In all cases, measured fully-turbulent heating levels agreed with each other to within the experimental uncertainty, although as discussed in the previous section, the discrete-trip heating were from 2% to 10% higher than the bowed panel levels. GASP heating levels were 5%-10% higher than the LAURA levels (and up to 15% higher near the nose) for all cases. As noted previously, the grid convergence error estimate for GASP was approximately 5% as compared to approximately 2% for LAURA. However, both sets of predictions matched the fully-turbulent experimental data to within the estimated experimental uncertainty of ±15% for all cases.

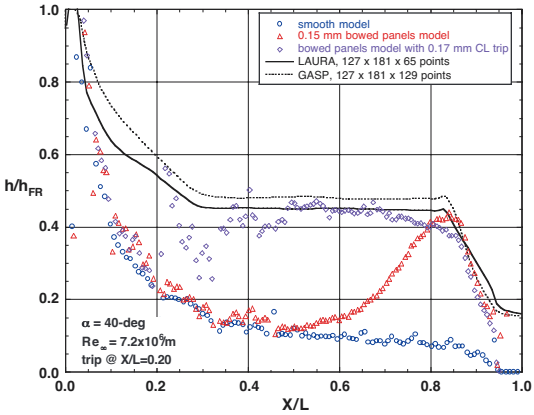

Figure 13: Comparison of Measured and Predicted Centerline Heating at $Re_\infty = 7.2x10^6$/m

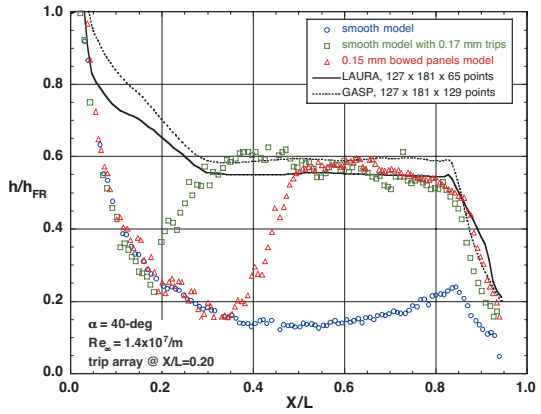

Figure 14: Comparison of Measured and Predicted Centerline Heating at $Re_\infty = 1.4x10^7$/m

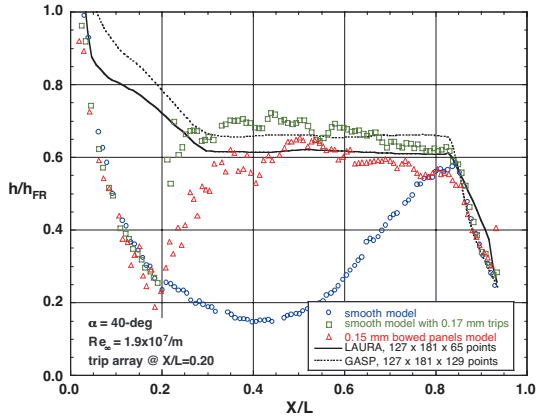

Figure 15: Comparison of Measured and Predicted Centerline Heating at $Re_\infty = 1.9x10^7$/m

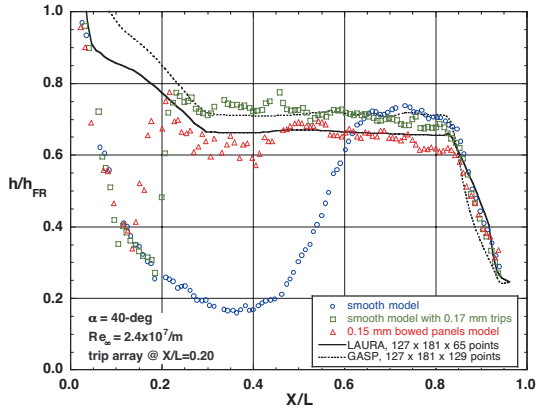

Figure 16: Comparison of Measured and Predicted Centerline Heating at $Re_\infty = 2.4x10^7$/m

Summary

An experimental and computational study of turbulent aeroheating on the X-33 vehicle has been conducted at perfect-gas air, Mach 6 wind tunnel conditions. Testing was conducted at α = 40-deg across a Reynolds number range of $0.72x10^7$/m to $2.4x10^7$/m ($2.2x10^6$/ft to $7.3x10^6$/ft) with 0.0132-scale models. Turbulent flow was generated on smooth test models and on models with discrete trips or bowed panels, and heating levels were measured using global phosphor thermography. Turbulent aeroheating predictions were performed using the Navier-Stokes solvers GASP and LAURA.

In the wind tunnel test, turbulent flow was produced by the trips and bowed panels at all but the lowest test Reynolds number, where both a trip and the bowed panels were required to produce turbulent flow, while turbulent flow was produced on the smooth models at only the highest Reynolds number. Turbulent aeroheating levels measured on all three model types agreed to within the estimated experimental uncertainty of ±15%, although levels on models with trips were generally slightly higher than on models with bowed panels. Large differences noted in previous studies between discrete trip and bowed panel heating levels were found to be due to a data acquisition system calibration error. For discrete trips, fully turbulent heating levels were shown to be independent of trip height for range of trips tested.

Computed turbulent heating levels agreed with each other to within 5%-10%, although GASP predictions were consistently higher than the LAURA predictions. Both sets of predictions matched the turbulent experimental data to within the estimated uncertainty for all test Reynolds numbers.

References

1. Bekey, I., Powell, R., and Austin, R., "NASA Studies Access to Space," Aerospace America, May 1994, pp. 38-43.

2. Cook, S. A., "X–33 Reusable Launch Vehicle Structural Technologies," AIAA Paper 97-10873, Nov. 1996.

3. Freeman Jr., D. C., Talay, T. A, and Austin, R. E., "Reusable Launch Vehicle Technology Program," AIAA Paper IAF 96-V.4.01, Oct., 1996.

4. Powell, R. W., Lockwood, M. K, and Cook, S. A., "The Road from the NASA Access-to-Space Study

to a Reusable Launch Vehicle," AIAA Paper IAF-98-V.4.02, Sept. 1998.

5. Baumgartner, R. I., and Elvin, J. D., "Lifting Body - An Innovative RLV Concept," AIAA Paper 95-3531, Sept. 1995.

6. Thompson, R. A., Hamilton II, H. H., Berry, S. A., and Horvath, T. J., "Hypersonic Boundary Layer Transition for X–33 Phase II Vehicle," AIAA Paper 98-0867, Jan., 1998.

7. Hamilton II, H. H., Weilmuenster, K. J., Berry, S. A., and Horvath, T. J., "Computational/ Experimental Aeroheating Predictions for X–33 Phase II Vehicle," AIAA Paper 98-0869, Jan. 1998.

8. Berry, S. A., Horvath, T. J., Hollis, B. R., Thompson, R. A., Hamilton II, H. H., "X–33 Hypersonic Boundary Layer Transition," *Journal of Spacecraft and Rockets*, Vol. 38, No. 5, pp. 646-657, Sept.-Oct. 2001.

9. Berry, S. A., Horvath, T. J., Kowalkowski, M. K., and Liechty, D. S., "X-33 (Rev-F) Aeroheating Results of Test 6770 in NASA Langley 20-Inch Mach 6 Air Tunnel," NASA TM-1999-209122, March 1999.

10. Hollis, B. R., Horvath, T. J., Berry, S. A., Hamilton H. H. II, Thompson, R. A, and Alter, S. J., "X-33 Computational Aeroheating Predictions and Comparison with Experimental Data," *Journal of Spacecraft and Rockets*, Vol. 38, No. 5, pp. 658-669, Sept.-Oct. 2001.

11. Hollis, B. R., Thompson, R. A., Murphy, K. J., Nowak, R. J., Riley, C. J., Wood, W. A., Alter, S. A., and Prabhu, R. K., "X-33 Aerodynamic Computations and Comparisons with Wind Tunnel Data," *Journal of Spacecraft and Rockets*, Vol. 38, No. 5, pp. 684-691, Sept.-Oct. 2001.

12. Horvath, T. J, Berry, S. A., Hollis, B. R., Liechty, D. S., Hamilton II, H. H., Merski, N. R., "X–33 Experimental Aeroheating at Mach 6 Using Phosphor Thermography," *Journal of Spacecraft and Rockets*, Vol. 38, No. 5, pp. 634-645, Sept.-Oct. 2001.

13. Murphy, K. J., Nowak, R. J., Thompson, R. A., Hollis, B. R., and Prabhu, R., "X–33 Aerodynamic Computations and Comparisons with Wind Tunnel Data," *Journal of Spacecraft and Rockets*, Vol. 38, No. 5, pp. 670-683, Sept.-Oct. 2001.

14. Thompson, R. A., "Review of X-33 Hypersonic Aerodynamic and Aerothermodynamic Development," 22nd International Congress of the Aeronautical Sciences, ICA-0323, Aug. 27 - Sept. 1, 2000.

15. Palmer, G., Kontinos, D., and Sherman, B., "Surface Heating Effects of X-33 Vehicle TPS Bowing, Steps, and Gaps," AIAA Paper 98-0865, Jan. 1998.

16. Prabhu, D. K., Wright, M. J., Marvin, J. G., Brown, J. L., and Venkatapathy, E., "X-33 Aerothermal Design Environment Predictions: Verification and Validation," AIAA Paper 2000-2686, June 2000.

17. Prabhu, D. K., Loomis, M. P., Venkatapathy, E., Polsky, S., Papadopoulos, P., Davies, C. B., and Henline, W. D., "X-33 Aerothermal Environment Simulations and Aerothermodynamic Design," AIAA Paper 98-0868, Jan. 1998.

18. Micol, J. R. "Hypersonic Aerodynamic/ Aerothermodynamic Testing Capabilities at Langley Research Center: Aerothermodynamic Facilities Complex," AIAA Paper 95-2107, June 1995.

19. Micol, J. R. "Langley Aerothermodynamic Facilities Complex: Enhancements and Testing Capabilities," AIAA Paper 98-0147, Jan. 1998.

20. Hollis, B. R., "Real-Gas Flow Properties for NASA Langley Research Center Aerothermodynamic Facilities Complex Wind Tunnels," NASA CR 4755, Sept. 1996.

21. Buck, G. M., "Automated Thermal Mapping Techniques Using Chromatic Image Analysis," NASA TM 101554, April 1989.

22. Buck, G. M., "Surface Temperature/Heat Transfer Measurement Using a Quantitative Phosphor Thermography System," AIAA Paper 91-0064, Jan. 1991.

23. Merski, N. R., "A Relative-Intensity, Two-Color Phosphor Thermography System," NASA TM 104123, Sept. 1991.

24. Merski, N. R., "Global Aeroheating Wind-Tunnel Measurements Using Improved Two-Color Phosphor Thermography Methods, *Journal of Spacecraft and Rockets*, Vol. 36, No. 2, pp. 160-170, March-April 1999.

25. Fay, J. A., and Riddell, F. R., "Theory of Stagnation Point Heat Transfer in Dissociated Air," *Journal of Aeronautical Sciences*, Vol. 25, No. 2., pp. 73-85, Feb. 1958.

26. Gnoffo, P. A., "An Upwind-Biased, Point-Implicit Algorithm for Viscous, Compressible Perfect-Gas Flows," NASA TP-2953, Feb. 1990.

27. Cheatwood, F. M., and Gnoffo, P. A., "User's Manual for the Langley Aerothermodynamic Upwind Relaxation Algorithm (LAURA)," NASA TM 4674, April, 1996.

28. Cheatwood, F. M., Merski, N. M., Riley, C. J., and Mitchletree, R. A., "Aerothermodynamic Environment Definition for the Genesis Sample Return Capsule," AIAA Paper 2001-2889, June 2001.

29. Roe, P. L., "Approximate Riemann Solvers, Parameter Vectors and Difference Schemes," *Journal of Computational Physics*, Vol. 43, No. 2, 1981, pp. 357-372.

30. Harten, A., "High Resolution Schemes for Hyperbolic Conservation Laws," *Journal of Computational Physics*, Vol. 49, No. 3, 1983, pp. 357-393.

31. Yee, H. C., "On Symmetric and Upwind TVD Schemes," NASA TM 88325, 1990.

32. Baldwin, B. S. and Lomax, H., "Thin Layer Approximation and Algebraic Model for Separated Turbulent Flow," AIAA Paper 78-257, Jan. 1978.

33. Cheatwood, F. M., and Thompson, R. A., "The Addition of Algebraic Turbulence Modeling to Program LAURA," NASA TM-107758, April 1993.

34. Dhawan, S., and Narashima, R., "Some Properties of Boundary Layer Flow from Laminar to Turbulent Motion," *Journal of Fluid Mechanics*, Vol. 1, Part 4, pp. 418-436, Jan. 1958.

35. AeroSoft, "GASP Version 3, The General Aerodynamic Simulation Program, Computation FLow Analysis Software for the Scientist and Engineer, User's Manual," Aerosoft Inc., Blacksburg, VA, May 1996.

36. Alter, S. J., The Volume Grid Manipulator (VGM): A Grid Reusability Tool," NASA CR-4772, April 1997.